**Superalloys 2012: 12th International Symposium on Superalloys**
*Edited by: Eric S. Huron, Roger C. Reed, Mark C. Hardy, Michael J. Mills, Rick E. Montero, Pedro D. Portella, Jack Telesman*
***TMS (The Minerals, Metals & Materials Society), 2012***

# EFFECT OF OFF-STOICHIOMETRY AND TERNARY ADDITIONS ON PLANAR FAULT ENERGIES IN $Ni_3Al$

K. V. Vamsi and S. Karthikeyan
Department of Materials Engineering, Indian Institute of Science, Bangalore-560012, INDIA

Keywords: First principles calculations, Stacking fault energy, Ni antisites, Titanium and Tantalum alloying

## Abstract

First principles calculations were done to evaluate the lattice parameter, cohesive energy and stacking fault energies of ordered γ′ ($L1_2$) precipitates in superalloys as a function of composition. It was found that addition of Ti and Ta lead to an increase in lattice parameter and decrease in cohesive energy, while Ni antisites had the opposite effect. Ta and Ti addition to stoichiometric $Ni_3Al$ resulted in an initial increase in the energies of $APB_{(111)}$, $CSF_{(111)}$, $APB_{(001)}$ and $SISF_{(111)}$. However, at higher concentrations, the fault energies decreased. Addition of Ni antisites decreased the energy of all four faults monotonically. A model based on nearest neighbor bonding was used for $Ni_3$(Al,Ta), $Ni_3$(Al, Ti) and $Ni_3$(Al, Ni) pseudo-binary systems and extended to pseudo-ternary $Ni_3$(Al,Ta,Ni) and $Ni_3$(Al,Ti,Ni) systems. Recipes were developed for predicting lattice parameters, cohesive energies and fault energies in pseudo-ternary systems on the basis of coefficients derived from simpler pseudobinary systems. The model predictions were found to be in good agreement with first principles calculations for lattice parameters, cohesive energies, and energies of $APB_{(111)}$ and $CSF_{(111)}$.

## Introduction

Ni-based superalloys owe their excellent high temperature properties to a high volume fraction of ordered and coherent γ′ precipitates in γ, which is an f.c.c. Ni solid solution [1]. The shear strength of the precipitate resulting from order strengthening, is the central reason for the excellent high temperature properties of Ni-base superalloys. The γ′ precipitate has a nominal composition of $Ni_3Al$ with an $L1_2$ structure. The morphology, lattice parameter, volume fraction, coarsening behavior and Stacking Fault Energies (SFE) of γ′ influence the high temperature strength and creep properties [2].

The primary glide dislocation in γ matrix has a Burgers vector of 1/2<110>{111}, and these dislocations are glissile at all temperatures [2]. Additionally, given the low stacking fault energy in the γ matrix, the 1/2<110> dislocations are often observed in extended configurations consisting of pairs of Shockley partial dislocations (of 1/6<112> type) separated by intrinsic stacking faults. The strength of the γ′ precipitates depends on the ease of their being sheared by matrix dislocations of 1/2<110> or 1/6<112> types. Such shearing is possible because the precipitate is coherent with the matrix. However, since the precipitate is ordered, 1/2<110> is not a lattice translation in γ′ and the passage of 1/2<110> superpartial dislocations is accompanied by the extension of Anti-Phase Boundaries (APB) on the (111) plane. Similarly the passage of 1/6<112> dislocations is associated with the extension of a Complex Stacking Fault (CSF) on the (111) plane. It is known that the 1/2<110> dislocations in screw orientations can cross-slip on to the (001) plane [3]. This phenomenon is accompanied by the formation of an APB on the (001) plane. This cube slip is closely associated with the formation of Kear-Wilsdorf locks which have an impact on yield anomaly in Ni-base superalloys [3]. The Superlattice Intrinsic Stacking Fault (SISF) is yet another fault that can be created by glide of dislocations, in this case, by the 1/3<112> Kear partial dislocations. The energies of these faults not only affect the resistance of γ′ to slip, but also to twinning – CSF and SISF energies are closely related to ease of twin transmission [4]. Additionally, the dislocation configurations into which a <110> superdislocation dissociates is strongly dependent on fault energies. In light of this, the aim of the present study was to probe the role of γ′ composition on the energies of $APB_{(111)}$, $CSF_{(111)}$, $APB_{(001)}$ and $SISF_{(111)}$.

Ni-base superalloys are based on the binary Ni-Al system. Commercial superalloys additionally contain up to 15 alloying elements, some of which (such as Co, Cr, Re, Ru, W, Mo) partition to γ, while others (such as Ta, Ti, Nb) partition to γ′[1]. The nominal composition of the γ′ precipitate is thus better described by $Ni_3$(Al,X) where X are various elements which substitute for Al in its sublattice. Ta and Ti are among the most important of these alloying elements: Ta in single crystal blade alloys and Ti in polycrystalline disk alloys [2]. Additionally, the γ′ precipitate is seldom stoichiometric − it is often Ni-rich with excess Ni populating the Al sublattice as antisites [5]. The presence of Ti, Ta and Ni in Al sublattice is expected to affect the lattice parameters, elastic properties and planar fault energies of the γ′ precipitate which will in turn affect the alloy's high temperature properties. The effect of composition on SFE has been extensively studied experimentally and computationally. Some of this data is summarized in Table 1. It is clear that SFE values reported are over a wide range. This is due to the variety of techniques used for evaluating SFE. Additionally, energies of all four faults have seldom been estimated by the same method and so consistent trends do not emerge. It is also noted that most alloys studied are model systems and the effect of γ′ composition has not been systematically studied over the range relevant to commercial superalloys. In this context, all four faults were systematically probed in this study via first principles electronic structure calculations using density functional theory. Calculations were done in the $Ni_3(Al_{1-(x+\delta)}X_xNi_\delta)$ system, where subscript *x* applies to ternary additions and *δ* represents off-stoichiometry related to Ni antisites. Three types of systems were studied:

(a) Ternary stoichiometric $Ni_3(Al_{1-x}X_x)$ with x=0 to1, δ=0 and X= Ti or Ta,
(b) Binary off-stoichiometric $Ni_3(Al_{1-\delta}Ni_\delta)$ with x=0 and δ=0 to 0.17, and
(c) Ternary off-stoichiometric $Ni_3(Al_{1-(x+\delta)}X_xNi_\delta)$ with x=0 to 0.3, δ=0 to 0.17 and X= Ti or Ta.

The third set of calculations closely mimics γ′ composition in commercial superalloys [6,7]. Simultaneous presence of both Ti and Ta was not explored.

## 2. Simulation Methodology

2.1. Computational details

Ab-initio density functional theory was used to calculate the ground state structural energies for perfect crystals and configurations containing faults [8,9]. Quantum Espresso [10] and Vienna Ab-initio Simulation Package (VASP) [11] codes were used. Quantum Espresso was used for calculations on ternary stoichiometric systems while VASP was used for calculations on binary and ternary off-stoichiometric systems. The plane wave kinetic energy cutoff of 680 eV was found to be optimal for the Quantum Espresso calculations. For VASP calculations, a kinetic energy cutoff of 400 eV was used. k point spacing was in the range of 0.19 $Å^{-1}$ to 0.20 $Å^{-1}$. Pseudopotentials based on Perdew-Burke-Ernzerhof Generalized Gradient Approximation (PBE-GGA) were employed [12]. Bulk properties of Ni, Al, Ti, Ta in their respective equilibrium structures were calculated to test the robustness of the pseudopotentials employed. Methfessel-Paxton first order spreading was used for Brillouin zone integration [13]. Calculations were first done on bulk systems to evaluate equilibrium lattice parameter and cohesive energy as a function of composition. Subsequently, faults were created in supercells (next section) whose dimensions were consistent with the equilibrium lattice parameter for the specific composition. Calculations were terminated when fault energies converged to within 1 $mJ/m^2$. Atomic relaxation was allowed in all calculations.

2.2 Supercell construction and fault energy calculation

Supercells of $L1_2$ were constructed in two different orientations. For calculating $CSF_{(111)}$, $APB_{(111)}$ and $SISF_{(111)}$ the basis vectors of the supercell were oriented along the [11-2], [-110] and [111] crystallographic directions. The stacking sequence of {111} planes in $L1_2$ is …|ABC|ABC|…The A, B and C layers are identical and in our supercell, each consisted of 6 Ni sites and 2 Al sites. Each layer was translated with respect to the one below by 1/6[11-2]. For calculating $APB_{(001)}$ the supercell was constructed with basis vectors along the [100], [010] and [001] crystallographic directions. The stacking sequence of (001) planes is …|A´B´|A´B´|… Here A´ and B´ layers are not identical; where layer A´ has 4 Ni sites and 4 Al sites, layer B contains 8 Ni sites. Figure 1 shows the (111) and (001) projections of atoms on two layers across which the fault is created. A fault was created by shearing the crystal between these adjacent layers by the shear vector appropriate to the fault (as indicated).

However, computationally, the fault was implemented not by shearing the supercell, but by adding the corresponding shear vectors to the periodic boundary repeat vectors of the computational cell. The number of atoms in the supercell was 48 for all the calculations such that the distance between the fault planes was more than 10Å (in both supercell orientations). The separation was sufficient to prevent interactions between the periodic images of the fault; interactions beyond 5Å are typically weak in metallic and intermetallic systems.

Quantum Espresso calculations in stoichiometric systems were done for 5 compositions ($Ni_3Al$, $Ni_3Al_{0.75}X_{0.25}$, $Ni_3Al_{0.5}X_{0.5}$, $Ni_3Al_{0.25}X_{0.75}$, $Ni_3X$) with X=Ti or Ta. Calculations were done on two unique configurations for all the intermediate compositions. The configurations were chosen in such a way that composition on the fault was maintained the same as in bulk. The fault energies were calculated as: $(E_{fault} - E_{perfect})/A$, where $E_{fault}$ is the energy of the faulted structure, $E_{perfect}$ is the energy of perfect structure and $A$ is the area of the faulted region in the supercell.

For VASP calculations in non-stoichiometric and ternary systems, γ´ compositions were such that ternary addition of Ni antisites or Ta/Ti were in dilute concentrations, and a large supercell would be needed to ensure that composition on the fault and the bulk were identical.

Table 1. A summary of stacking fault energies in $Ni_3(Al_{1-(x+\delta)}X_xNi_\delta)$ reported in literature (in $mJ/m^2$).

| Composition | Type of calculation | $APB_{(111)}$ | $APB_{(001)}$ | $CSF_{(111)}$ | $SISF_{(111)}$ | References |
|---|---|---|---|---|---|---|
| $Ni_3Al$ | *ab-initio* | 240 | 137 | 308 | 147 | [14] |
| | | 175 | 140 | 225 | 40 | [15] |
| | EAM | 142 | 83 | 121 | 13 | [16] |
| | | 252 | 80 | 202 | 51 | [17] |
| | exp. | 111±15 | 90±15 | | 10±5 | [18] |
| | | 195±13 | 160±20 | 236±29 | | [19] |
| Ni-22Al | exp. | 175±15 | 104±15 | 235±40 | | [20] |
| Ni-22.9Al | exp. | 169±19 | 104±8 | | | [21] |
| Ni-24Al | exp. | 176±11 | 135±18 | 206±27 | | [19] |
| Ni-24.2Al | exp. | 163±21 | 122±11 | | | [21] |
| Ni-25.9Al | exp. | 190±26 | 170±21 | | | |
| Ni-26Al | exp. | 219±17 | 184±16 | 277±49 | | [19] |
| $Ni_3Ti$ | *ab-initio* | 550 | -160 | | | [15] |
| Ni-17.4Al-6.2Ti | exp. | 250±30 | 250±30 | | | [22] |
| Ni-16.67Al-8.33Ti | *ab-initio* | 476 | | | | [23] |
| Ni-12.5Al-12.5Ti | *ab-initio* | 633 | | | | |
| Ni-8.33Al-16.67Ti | *ab-initio* | 624 | | | | |
| Ni-24.7Al-1Ta | exp. | 237±30 | 200±25 | | | [24] |
| | | | | 352±50 | | [25] |
| Ni-16.67Al-8.33Ta | *ab-initio* | 540 | | | | [23] |
| Ni-12.5Al-12.5Ta | *ab-initio* | 443 | | | | |
| Ni-8.33Al-16.67Ta | *ab-initio* | 238 | | | | |

To avoid the computational cost associated with this, the following procedure was followed: a supercell of 48 atoms was chosen and a dilute substitution was made in the Al sublattice (as shown in Figure 2). A series of calculations were done, wherein the fault was created between each pair of planes (the planes shown in the schematic are of (111) type). Such a creation of the fault on planes 1-6 resulted in six unique fault configurations whose energy was computed using DFT. For each configuration, the ternary addition was either on the fault plane or away from it by a specific distance. By assuming that in experiments, the stacking fault created during shearing of γ′ could conform to any of these six configurations, the fault energy was computed as the statistical average of the fault energies for each of the six configurations (for a given composition). This procedure is identical to constructing a supercell that is six times larger.

.

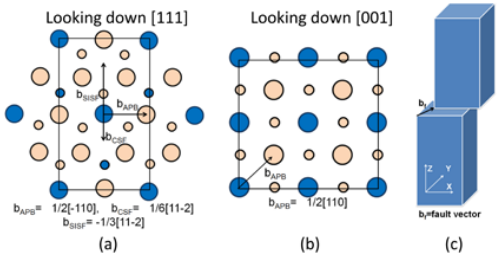


Figure 1. Projection of atoms on the (a) (111) and (b) (001) plane. The dark blue circles represent atoms in the Al-sublattice while light brown circles represent atoms in Ni sublattice. The smaller and larger atoms lie on two adjacent planes across which the fault is created. Figure 1(c) shows a schematic of fault creation with fault vector, $b_f$ corresponding to vectors indicated in (a) and (b).

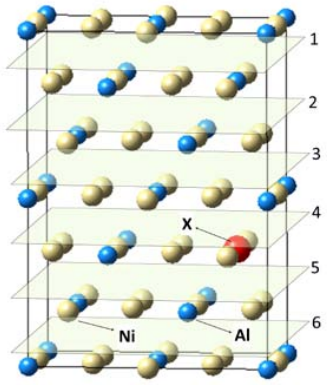


Figure 2. Schematic showing the creation of series of faults at locations 1-6.

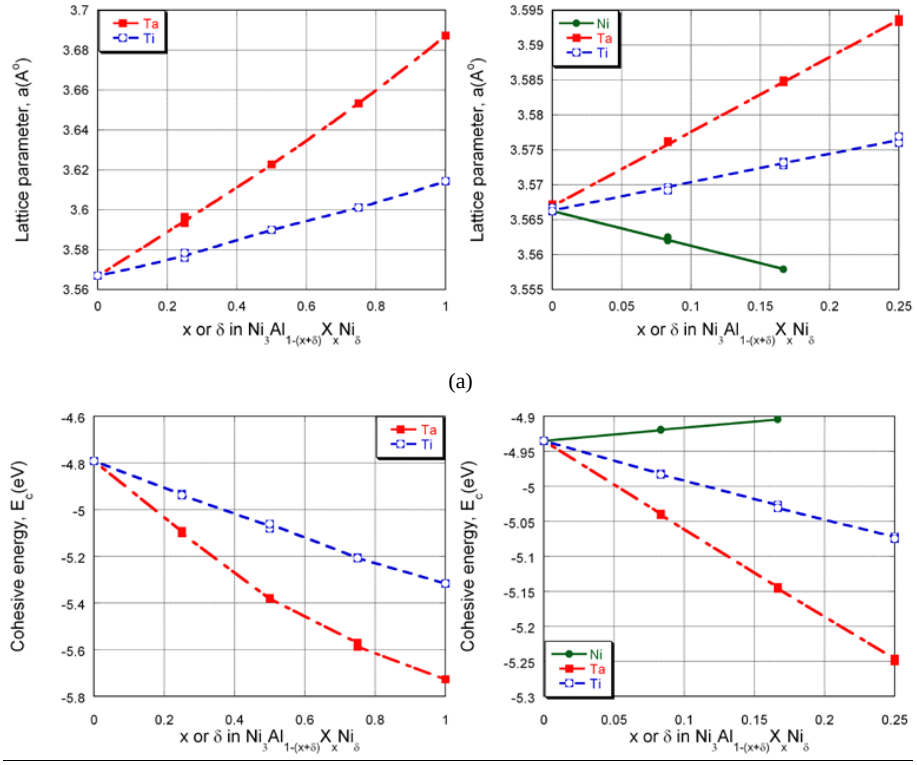


Figure 3. Variation of (a) lattice parameter and (b) cohesive energy with Ti/Ta or Ni antisite addition. The plots to the right show only the dilute solution regime. The fit parameters in Table 4 are derived from (b),(d),(f) and (h).

Table 2. A summary of fault energies (in $mJ/m^2$) calculated in this study for the various compositions. Experimental values for γ′ with similar composition are also indicated in brackets where available. The reference for the experimental data is also shown.

| Composition | $CSF_{(111)}$ | $APB_{(111)}$ | $APB_{(001)}$ | $SISF_{(111)}$ | Ratio of $APB_{(111)}$ to $APB_{(001)}$ | Reference |
|---|---|---|---|---|---|---|
| $Ni_3Al$ | 170 (236) | 152 (195) | 58 (160) | 39 | 2.62 | [19] |
| $Ni_3Al_{0.917}Ni_{0.083}$ | 138 | 98 (169) | 7 (104) | 20 | 14.00 | [21] |
| $Ni_3Al_{0.833}Ni_{0.167}$ | 109 | 45 | -6 | 11 | - | |
| $Ni_{3.083}Al_{0.833}Ta_{0.083}$ | 174 | 145 | 42 | 37 | 3.45 | |
| | 181 | 140 | 56 | 49 | 2.50 | |
| $Ni_{3.083}Al_{0.833}Ti_{0.083}$ | 167 | 142 | 37 | 47 | 3.84 | |
| | 168 | 127 | 56 | 55 | 2.27 | |
| $Ni_3Al_{0.917}Ta_{0.083}$ | 227 | 210 | 144 | 90 | 1.46 | |
| $Ni_3Al_{0.833}Ta_{0.167}$ | 295 | 281 | 230 | 147 | 1.22 | |
| $Ni_3Al_{0.75}Ta_{0.25}$ | 388 | 378 | 306 | 203 | 1.24 | |
| | 376 | 370 | 298 | 196 | 1.24 | |
| | 396 | 326 | 344 | 194 | 0.95 | |
| $Ni_3Al_{0.5}Ta_{0.5}$ | 608 | 473 | 332 | 73 | 1.42 | |
| | 599 | 476 | 288 | 127 | 1.65 | |
| $Ni_3Al_{0.25}Ta_{0.75}$ | 106 | -61 | -521 | -465 | 0.12 | |
| $Ni_3Ta$ | -450 | -691 | -1204 | -1166 | 0.57 | |
| $Ni_3Al_{0.917}Ti_{0.083}$ | 213 | 194 | 135 | 91 | 1.44 | |
| $Ni_3Al_{0.833}Ti_{0.167}$ | 246 | 217 | 204 | 130 | 1.06 | |
| $Ni_3Al_{0.75}Ti_{0.25}$ | 298 | 249 | 244 | 174 | 1.02 | |
| | 313 | 300 | 243 | 176 | 1.24 | |
| | 299 | 242 (250) | 254 (250) | 159 | 0.95 | [22] |
| $Ni_3Al_{0.5}Ti_{0.5}$ | 444 | 529 | 370 | 232 | 1.43 | |
| | 451 | 404 | 394 | 221 | 1.02 | |
| $Ni_3Al_{0.25}Ti_{0.75}$ | 602 | 578 | 379 | 161 | 1.52 | |
| | 631 | 527 | 377 | 155 | 1.40 | |
| $Ni_3Ti$ | 468 | 360 | 51 | -127 | 7.12 | |

## 3. Results

3.1 Bulk properties

Figure 3a shows the variation of lattice parameter with replacement of Al with ternary Ti/ Ta or with Ni antisites. Figure 3b shows the effect on cohesive energy. The calculated values of lattice parameter of $Ni_3Al$ and $Ni_3Ti$ ($L1_2$) match well with values in literature [26,27]. Cohesive energy of $Ni_3Al$ is also in good agreement with experiments [28]. Both Ta and Ti increase the lattice parameter of $Ni_3(Al_{1-x}X_x)$ with a nearly linear dependence; Ta has the larger effect. Introduction of Ni-antisites decreases the lattice parameter linearly. While the addition of Ta and Ti decreases the cohesive energy, introduction of Ni-antisites increases it.

3.2 Planar fault energies

Table 2 provides a summary of fault energies calculated in this study for the various compositions. Figure 4 shows the trends with respect to composition for each of the four faults − the left panel shows results for concentrated ternary stoichiometric systems, while the figures in the right panel show results for dilute ternary stoichiometric and binary non-stoichiometric systems. Figures 4(a) and (b) show the variation of APB energy on the (111) plane. The addition of Ti and Ta leads to an increase in APB energy up to intermediate compositions. Ta has a stronger effect in increasing the APB energy. The fault energy reaches a maximum at x=~0.5 for Ta and ~0.75 for Ti, beyond which it drops. In fact, in the case of Ta, for x>0.8, the APB energy becomes negative suggesting that creation of the fault is energetically favorable.

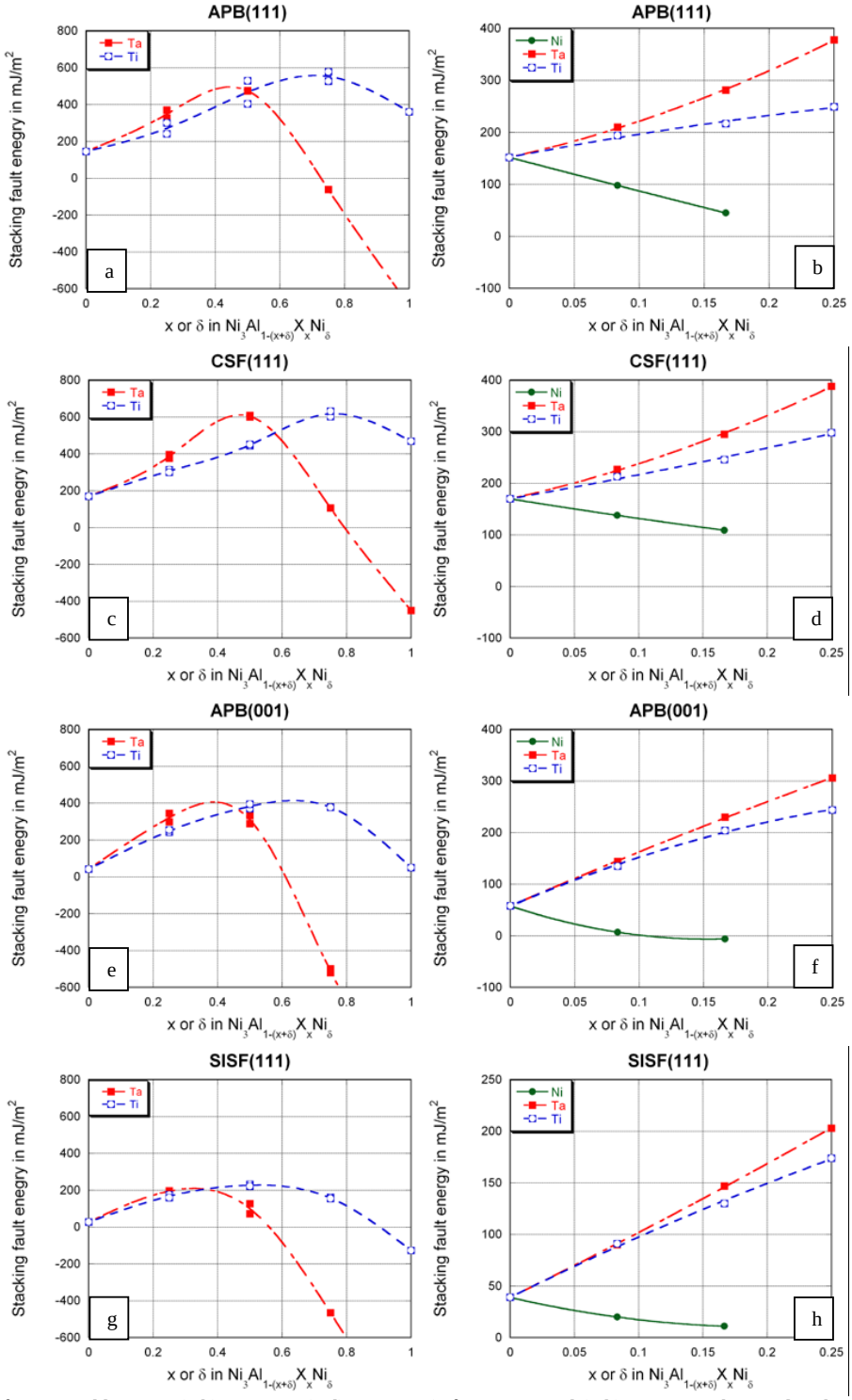


Figure 4. Effect of ternary addition on (a-b) $APB_{(111)}$, (c-d) $CSF_{(111)}$, (e-f) $APB_{(001)}$ and (g-h) $SISF_{(111)}$. The panel to the right is for dilute compositions. The fit parameters in Table 4 are derived from (b),(d),(f) and (h).

The introduction of Ni antisites results in a decrease in APB energy as seen from Figure 4b. In this case, the dependence of fault energy is monotonic.

The qualitative trends are similar for the case of the other faults as well (Figures 4c-4h). The significant differences between the energies of the various faults are highlighted here. A key difference between the faults is in the magnitude of their energy. In general, $CSF_{(111)} > APB_{(111)} > APB_{(001)} > SISF_{(111)}$. The only exception to this is the energy of $SISF_{(111)} > APB_{(001)}$ when Ni antisites substitute for Al (Figures 4 and Table 2). It should be noted that while all faults have a negative energy for high concentrations of Ta, only the $SISF_{(111)}$ has a negative energy for high concentrations of Ti. The composition at which the maximum in fault energy occurs shifts to more dilute compositions for $SISF_{(111)}$ and $APB_{(001)}$. The reasons for these observations are discussed in the next section.

## 4. Discussion

4.1. Binary and ternary stoichiometric systems

In these systems, there are two occupants in the Al sub-lattice: Al and Ni in the case of binary non-stoichiometric systems, and Al and Ta/Ti in the case of ternary stoichiometric systems. Hence these systems can be treated as pseudo-binary with a fixed Ni level in the Ni sublattice and a nominal composition of $Ni_3(Al_{1-m}M_m)$. The element M is either Ti/Ta (and $m = x$) or Ni in off-stoichiometric binary γ′ (and $m = \delta$)

4.1.1. Bulk properties

Both Ta and Ti increase the lattice parameter suggesting that atoms of these elements are larger than that of Al. Ni, which causes a decrease in lattice parameter, is smaller than Al. These results are consistent with what has been reported in the literature [29]. A linear dependence of lattice parameter on composition suggests that Vegard's law is applicable. As a result, lattice parameter, $a$, for any pseudo-binary composition can be written as: $a = a_0 + \alpha_M \cdot m$, where $a_0$ is the lattice parameter of binary stoichiometric $Ni_3Al$, $\alpha_M$ is the Vegard's coefficient for element M and $m$ is the composition of M in the Al sublattice. The linear fit is shown in Figure 3a for dilute compositions.

Lattice parameter calculations were done to generate the stress-free supercell dimensions. These calculations were also necessary for determining the area of the stacking fault, which in turn is used for computing SFE. Additionally, the effect of composition on lattice parameter is of importance in the determination of misfit between γ and γ′. The sign and magnitude of misfit between the phases is known to control microstructural evolution during creep (i.e., rafting) and hence the creep behavior [30,31]. A comprehensive study of the effects of alloying (i.e., Co, Cr, Ta, Ti, Al, W, Mo, Re, Ru, etc.) on lattice parameters of γ and γ′ using first principles calculations is currently underway.

Addition of both Ta and Ti decreases the cohesive energy. A lower negative cohesive energy implies stronger bonding. The effect of Ta and Ti are due to the fact that these additions contribute extra d-electrons which result in enhanced bonding and a lowering of the cohesive energy. Addition of Ni antisites, however, reduces the extent of ordering and the fraction of strong Ni-Al bonds, resulting in an increase of cohesive energy. Once again the dependence of cohesive energy on composition is nearly linear. This is expected given that the number of electrons contributing to bonding scales linearly with concentration (to a first order approximation). So $E_c$, the cohesive energy for any pseudo-binary composition can be written as:
$E_c = E_{c,0} + \beta_M \cdot m$, where $E_{c,0}$ is the cohesive energy of binary stoichiometric $Ni_3Al$, $\beta_M$ is linear coefficient for element M. The linear fit is shown in Figure 3b for dilute compositions.

4.1.2. Fault energies

Creation of stacking faults is associated with local changes in structure and bonding environment. The energy of the fault is thus related to the difference in the total bond energy of the system before and after creation of the fault. Formation of faults is also associated with strain energy and this too contributes to the total fault energy. However, this contribution has been estimated to be <10% and detailed results will be presented elsewhere [32]. Within the scope of this paper, we attempt to understand the observed trends in fault energies on the basis of only the changes in bonding environment resulting from faulting. As a first-order approximation, a nearest neighbor bond (i.e., a quasichemical approach) can be invoked to qualitatively explain these trends. In such an approach, the energy of the system (either perfect or faulted) is the sum of bond energies between neighboring atoms. The bonds can be considered to be due to purely pair-wise interactions. One can include interactions between not only the first nearest neighbors (FNN), but also second (SNN), third (TNN) and so on and thus make the model more precise. For atoms adjacent to the stacking fault plane, creation of the fault is accompanied by loss of certain types of bonds and a gain of certain others, at FNN, SNN and TNN distances. This change in bonding environment is summarized in Table 3.

Table 3. Average change in bonding environment per atom on the fault plane in stoichiometric $Ni_3Al$

| Distance | Type | $SISF_{(111)}$ | $APB_{(001)}$ | $APB_{(111)}$ | $CSF_{(111)}$ |
|---|---|---|---|---|---|
| a/√2 (FNN) | (Al-Al) | – | – | 0.125 | 0.125 |
| | (Ni-Al) | | | -0.25 | -0.25 |
| | (Ni-Ni) | | | 0.125 | 0.125 |
| a (SNN) | (Al-Al) | – | -0.125 | -0.375 | -0.375 |
| | (Ni-Al) | | 0.25 | 0.75 | 0.75 |
| | (Ni-Ni) | | -0.125 | -0.375 | -0.375 |
| 2a/√3 (TNN) | (Al-Al) | 0.125 | – | – | 0 |
| | (Ni-Al) | 0 | | | 0.25 |
| | (Ni-Ni) | 0.375 | | | 0.25 |

The creation of an $SISF_{(111)}$ results in a local change in the stacking sequence of (111) planes and the local structure across the fault is hexagonal (not cubic). Despite this, $SISF_{(111)}$ creation does not result in FNN and SNN violations for atoms on the fault plane; violations start with the TNN bonds (Table 3). Since TNN interactions are expected to be much weaker than FNN and SNN interactions, the energy of the SISF is small. The creation of $APB_{(001)}$ does not change the stacking sequence, but still results in a change in bonding environment. In this case, there are no FNN violations; violations start at the SNN distance (Table 3). Given that SNN interactions are stronger than TNN interactions, the $APB_{(001)}$ energy is greater than the $SISF_{(111)}$ energy. There is no change in stacking sequence due to creation of $APB_{(111)}$ either. However, violations begin right from the FNN distance (Table 3) and so one expects the energy of $APB_{(111)}$ > energy of $APB_{(001)}$. Note that there are no TNN violations in the case of $APB_{(111)}$. In the creation of $CSF_{(111)}$, there is a change in stacking sequence and violations start with the FNN interaction. Additionally, there are

TNN violations (Table 3). As a consequence, for a given composition, fault energies display the following trend: $SISF_{(111)}$< $APB_{(001)}$< $APB_{(111)}$< $CSF_{(111)}$.

A quasi-chemical model based on nearest neighbor violations (i.e., regular solution model) was developed to explain the effect of pseudo-binary additions of M (i.e. Ti/Ta or Ni) on fault energies. In this model, fault energy was expressed in terms of the number and type of neighbor violations, pairwise strengths of Ni-Ni, Ni-Al, Ni-M, Al-Al, Al-M, M-M bonds at different distances and *m*, the amount of ternary addition. A simplification invoked was the consideration of only those violations that are most relevant to the fault, such as FNN violations for $APB_{(111)}$ and $CSF_{(111)}$, SNN violations for $APB_{(001)}$ and TNN violations for $SISF_{(111)}$. The full development of the model is presented elsewhere [32]. The model predicted that in the dilute limit, stacking fault energy for any fault in the pseudo-binary $Ni_3(Al_{1-m}M_m)$ could be expressed by a second order polynomial of form: $\gamma_0^f = \gamma_{0+}(\chi_{1,M})\cdot m+(\chi_{2,M})\cdot m^2$ where $\gamma_0$ is the fault energy of the fault in binary stoichiometric $Ni_3Al$ and $\chi_{1,M}$ and $\chi_{2,M}$ are first and second order coefficients for element M. The values of these coefficients are given for the four faults in Table 4. The coefficients were derived from fitting a second order polynomial to the fault energies in Figures 4 b, d, f, h.

As is clear from Figure 4, addition of Ta or Ti increases the $APB_{(111)}$ and $CSF_{(111)}$ energies in dilute concentrations. One can explain this by accounting for bond violations in these faults. In binary $Ni_3Al$, there is a gain of unfavorable Al-Al and Ni-Ni FNN bonds at the expense of favorable Ni-Al bonds (Table 3). When a ternary element, for instance, Ta, is present, a fraction of the bonds lost are of Ni-Ta type and these bonds are stronger than Ni-Al bonds, as is clear from the higher cohesive energy of $Ni_3Ta$ than $Ni_3Al$ in all geometric close packed structures (Table 5). This results in a greater energy penalty for creating $APB_{(111)}$ and $CSF_{(111)}$ in alloys containing Ta or Ti. Addition of Ni, however, reduces these energies. It is easy to explain this using similar arguments: a fraction of bonds lost are of Ni-Ni type and these bonds are weaker than Ni-Al bonds. In the limit where the antisite concentration is so large that the system is effectively disordered, energy of $APB_{(111)}$ becomes zero and $CSF_{(111)}$ is identical to intrinsic stacking fault energy of the disordered system.

In the case of $APB_{(001)}$, favorable Al-Al and Ni-Ni bonds are lost and unfavorable Al-Ni bonds are gained at the SNN distance (Table 3). When Ta (or Ti) is present, a fraction of bonds lost are of Al-Ta (or Al-Ti) type. The Al-Ta (or Al-Ti) bonds at the SNN distance are stronger than Al-Al bonds at the same distance. This is evident in Figure 5, which shows the enthalpy of mixing in the pseudobinary $Ni_3(Al_{1-m}M_m)$. In perfect $L1_2$ structure, the shortest Al-M, Al-Al and M-M type bonds are at the SNN distance. The negative enthalpy of mixing in $Ni_3$(Al, Ta) and $Ni_3$(Al, Ti) is indicative of stronger Al-Ta and Al-Ti bonds than Al-Al bonds at the SNN distance. One can explain the decrease in $APB_{(001)}$ with addition of Ni antisites using similar arguments. The local stacking sequence about the $SISF_{(111)}$ is …|AB|AB|… So the creation of the fault results in Ni-Ni and M-M bonds at a distance of $(2a/\sqrt{3})$. This is the distance between the two nearest A layers on either side of the fault; bonds are absent at this distance in perfect $L1_2$ structure. It is likely that the increase in SISF energy with the addition of ternary element is due to unfavorable M-M or Ni-Ni bonds at this distance.

A direct consequence of the dependence of fault energy on composition is that based on the composition of γ′, it is likely that the ternary additions or the Ni antisites will desegregate or segregate to the fault to reduce the overall fault energy. Such effects may lead to strengthening via Suzuki drag mechanisms.

Table 4. Coefficients for lattice parameter, cohesive energy and fault energies derived from pseudobinary data in the dilute solution range. The linear coefficients are in units per (at.frac). The second order coefficients are in units per $(at.frac)^2$

| Property | Ternary addition | Coefficients | | |
|---|---|---|---|---|
| | | $a_0$ (Å) | $\alpha_M$ | |
| Lattice parameter | Ni | 3.5662 | -0.0500 | |
| | Ti | | 0.0416 | |
| | Ta | | 0.1076 | |
| | | $Ec_0$ (eV/atom) | $\beta_M$ | |
| Cohesive energy | Ni | -4.9353 | 0.1845 | |
| | Ti | | -0.5536 | |
| | Ta | | -1.252 | |
| | | $\gamma_0$ (mJ/m$^2$) | $(\chi_{1,M})$ | $(\chi_{2,M})$ |
| $CSF_{(111)}$ | Ni | 170 | -402 | 216 |
| | Ti | | 439 | 269 |
| | Ta | | 552 | 1269 |
| $APB_{(111)}$ | Ni | 152 | -654 | 72 |
| | Ti | | 485 | -413 |
| | Ta | | 556 | 1379 |
| $APB_{(001)}$ | Ni | 58 | -840 | 2736 |
| | Ti | | 1072 | -1292 |
| | Ta | | 1079 | -341 |
| $SISF_{(111)}$ | Ni | 39 | -288 | 720 |
| | Ti | | 617 | -322 |
| | Ta | | 609 | 193 |

Table 5. Comparison of cohesive energies (eV/atom) of $Ni_3Al$, $Ni_3Ti$, $Ni_3Ta$ in various geometrically close packed structures.

| Compositions | Structure | | | | |
|---|---|---|---|---|---|
| | $L1_2$ | $DO_{22}$ | $DO_{24}$ | $DO_{19}$ | $DO_a$ |
| $Ni_3Al$ | -4.9363 | -4.9158 | -4.9203 | -4.9256 | -4.9129 |
| $NI_3Ti$ | -5.4453 | -5.4098 | -5.4583 | -5.4458 | -5.4031 |
| $Ni_3Ta$ | -5.9172 | -6.0888 | -6.0027 | -6.0648 | -6.0718 |

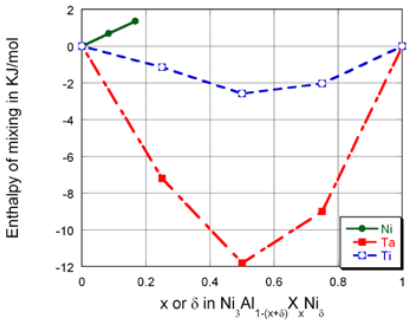


Figure 5. Effect of Ta, Ti and Ni addition on enthalpy of mixing in $Ni_3(Al_{1-m}M_m)$

While trends are monotonic for Ni antisite addition, all fault energies exhibit a maximum value in the case of Ti or Ta addition. The reasons for this are likely related to the fact that there is enhanced Ti-Ti and Ta-Ta type interactions at high concentrations, and loss or gain of bonds of this type counter the effects due to loss or gain of Ni-Ti and Ni-Ta bonds. It should also be noted that a pairwise interaction model is not very robust in accounting for interactions in metallically bonded systems. It is well known that strength of metallic bonds depend on local environment [33]. These details need to be incorporated into a more complete model to understand trends at high concentrations of the ternary addition.

It should be noted that $Ni_3Ti$ is most stable in the $D0_{24}$ structure (Table 5). This structure consists of …|AB|AB|… stacks of close packed planes that are identical to the close packed planes in $L1_2$. The creation of an $SISF_{(111)}$ generates a local structure that is identical to $D0_{24}$. This suggests that when one creates an $SISF_{(111)}$ in $Ni_3Ti$ that is initially in $L1_2$ structure, the local configuration about the fault is actually that of the stabler crystal structure, hence the negative $SISF_{(111)}$ energy for $Ni_3Ti$. In the case of $Ni_3Ta$ too, it is clear that $D0_{24}$ has a lower energy than $L1_2$, again resulting in negative SISF energy. Similarly, the creation of $APB_{(001)}$ results in a local structure that is identical to the $D0_{22}$ structure. Since $Ni_3Ta$ is stabler in $D0_{22}$ than in $L1_2$ (Table 5), the energy of $APB_{(001)}$ is negative for $Ni_3Ta$.

4.2. Ternary non-stoichiometric systems

First principles calculations were also employed in more complex ternary non-stoichiometric systems wherein the Al sublattice was occupied by three species: either Al, Ta and Ni, or Al, Ti and Ni. The calculated fault energies for these are also listed in Table 2. These systems constitute pseudo-ternary systems and are close to actual γ′ compositions in commercial superalloys. In an attempt to explain the fault energies obtained from these calculations, each of these pseudo-ternary system was in turn modeled on the basis of the two pseudo-binary systems, i.e., the $Ni_3(Al_{1-(x+\delta)}X_xNi_\delta)$ was modeled on the basis of $Ni_3$(Al, X) and $Ni_3$(Al, Ni) systems. This treatment is akin to a ternary regular solution model built on pairwise interactions. It ignores Al-Ni-X type three component interaction terms. Additionally, for simplicity, Ni-X type interactions in the Al sublattice were also ignored and so the model is strictly valid only for dilute levels of $x$ and $\delta$. Using such a model one can predict the lattice parameter, cohesive energy and energy of all the faults. For example, in the $Ni_3(Al_{1-(x+\delta)}Ta_xNi_\delta)$ system,

$$a = a_{0+}\ \alpha_{Ta}\cdot x+\alpha_{Ni}\cdot\delta;$$

$$E_c = E_{c,0+}\ \beta_{Ta}\cdot x+\beta_{Ni}\cdot\delta;$$

$$\gamma_0^f = \gamma_{0+}\ (\chi_{1,Ta})\cdot x+(\chi_{2,Ta})\cdot x^2+\ (\chi_{1,Ni})\cdot\delta+(\chi_{2,Ni})\cdot\delta^2$$

Using this model which employs coefficients derived from pseudo-binary calculations (presented in the previous section, Table 4), one can predict lattice parameters, cohesive energies and fault energies in ternary non-stoichiometric systems. Comparisons between the predicted value and the value derived from first principles calculations (for two atomic configurations) are shown in Figure 6 and Figure 7. It is clear that the predicted values are in very good agreement with the calculated value for both lattice parameter and cohesive energy in $Ni_3(Al_{1-(x+\delta)}Ta_xNi_\delta)$ and $Ni_3(Al_{1-(x+\delta)}Ti_xNi_\delta)$ (Figure 6). The predicted values are in good agreement and within 10% error of the calculated values for $APB_{(111)}$ and $CSF_{(111)}$. It should be noted that 10% is acceptable in the context of fault energies. The variation in fault energies between different configurations (but same composition) can be up to 20%. Additionally, the margin of error in experiments is even larger, sometimes up to 30%.

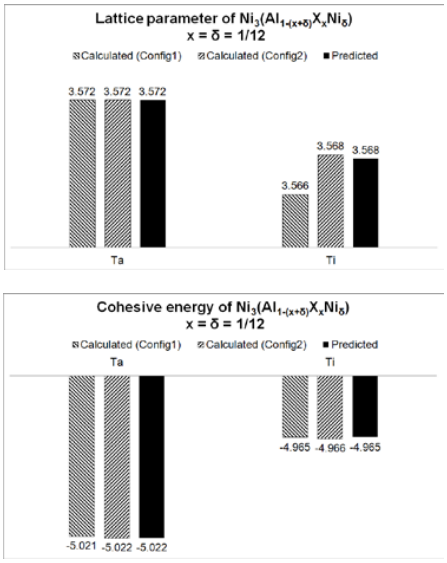


Figure 6. Comparison of lattice parameters (top) and cohesive energies (bottom) between calculated (from first principles, hashed bars) and predicted values (from coefficients derived from pseudo-binary calculations, solid bars).

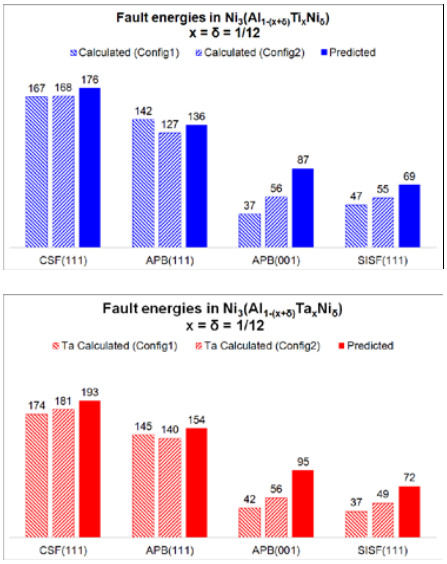


Figure 7. Comparison of fault energies between the calculated (from first principles, hashed bars) and predicted values (from coefficients derived from pseudo-binary calculations, solid bars). The calculations were done on two configurations each for $Ni_3(Al_{1-(x+\delta)}Ti_xNi_\delta)$ (top) and $Ni_3(Al_{1-(x+\delta)}Ta_xNi_\delta)$ (bottom).

However, the predicted values for the case of $APB_{(001)}$ and $SISF_{(111)}$ are 50-100% in error. The error is systematic: the predicted values are consistently higher than the calculated values, suggesting that the error stems from the simplifications of the model. A likely source of this error is that three-component interactions, as well as Ni (antisite)-X interactions are ignored in the current model. It is presumable that for faults such as $APB_{(001)}$ and $SISF_{(111)}$, where violations begin only at the SNN, and for which long range interactions affect fault energies, the assumed dilute solution model is inadequate. While the dilute solution model appears to be valid for $APB_{(111)}$ and $CSF_{(111)}$, it is important to establish the composition limits where the model breaks down and errors in predicted values become unacceptable. Work in this direction is currently underway.

4.3. Implications on mechanical properties

Precipitate shear is an important deformation mechanism in blade alloys at low temperatures and high stresses (typically 750 MPa and 750 °C to 850 °C). In this regime, several faulted configurations, including SISF and APB, have been observed during primary creep regime [34]. It has also been reported that Ta suppresses the extent of primary creep [35]. This is likely due to the increased strength of the precipitate. This is consistent with our calculations, which show a sharp increase in fault energies with the addition of Ta; precipitate strength scales linearly with stacking fault energy. Since shearing is primarily by 1/2<110> or by a pair of 1/6 <112>, the enhanced $APB_{(111)}$ and $CSF_{(111)}$ energies result in strengthening.

Order strengthening is perhaps even more important in disk alloys containing Ti where a variety of precipitate shear mechanisms have been reported over a range of temperatures and stresses [4]. The beneficial effect of Ti towards order strengthening has been previously reported [36] and our findings that Ti increases fault energies are consistent with this. Lastly, it is well documented that high temperature strength of $Ni_3Al$ is superior to that of $Ni_{3+\delta}Al$ [37]. This again is consistent with the lowering of fault energies in off-stoichiometric $Ni_{3+\delta}Al$ as evidenced in our calculations.

In several disk alloys, including Rene 88DT and Rene 104, microtwinning has been observed at high stresses and low temperatures [4]. The mechanism is significant in that it is associated with low creep rates. Such twinning, also called pseudotwinning, is caused by repeated passage of 1/6<112> type partial dislocations on parallel and adjacent (111) planes in the matrix and in γ′. Our calculations suggest that Ti addition leads to an increase in CSF energy on (111) and this is expected to make pseudotwinning difficult. However, it should be noted that at relatively high levels of Ti or Ta [See Figure 4], there is a sharp decrease in the SISF energy. This suggests that in γ′ with such compositions, 1/3[11-2] type Kear partial dislocations could become active in γ′ and result in enhanced true-twinning.

It is well-known the high temperature capability of Ni-base superalloys is closely related to the phenomenon of yield anomaly wherein an increase in yield strength with temperature is observed. This phenomenon is understood in terms of the formation of Kear-Wilsdorf locks [3] in γ′ that result from the cross-slip of 1/2<110> screw dislocations from {111} planes to {001} planes, followed by their dissociation into sessile configurations. The passage of an ordinary matrix dislocation results in the formation of APBs on the glide plane. Cross-slip from {111} to {001} is promoted if the APB energy on the {001} plane is sufficiently smaller than that on the {111} plane. Paidar et al. have proposed that cross-slip from {111} to {001} occurs when the ratio of fault energies, $APB_{(111)}/APB_{(001)} > \sqrt{3}$ [38]. Yoo et al. [39] have proposed a modified criterion incorporating elastic anisotropy where it is suggested that cross-slip occurs when $(1+f_1\sqrt{2})\ APB_{\{111\}}/APB_{\{010\}} > \sqrt{3}$, where $f_1$ is the anisotropy factor given by $\sqrt{2}(A-1)/(A+2)$ and $A$ is Zener's ratio of elastic anisotropy given by: $A=2C_{44}/(C_{11}-C_{12})$. In the absence of data on elastic anisotropy, one assumes isotropy and Paidar's criterion is recovered. Table 2 shows the ratio of $APB_{(111)}/APB_{(001)}$ from our calculations. It is evident that this criterion is readily satisfied for binary $Ni_3Al$. An increase in off-stoichiometry increases the ratio suggesting the possibility of enhanced cross-slip. It is also clear that ternary Ti or Ta additions results in fault energies which do not satisfy the criterion and in those cases yield anomaly is not expected. Dimiduk [21] have previously calculated the ratio of APB energies for a variety of ternary additions and found that the ratio was in the range 0.98 to 1.63. Our results are consistent with these observations. If Ni-antisites are also present in addition to the ternary element, it is likely that the ratio will be higher and cross-slip can be promoted.

## 5. Conclusions

First principles calculations were done to evaluate lattice parameter, cohesive energy and stacking fault energies of ordered $Ni_3(Al_{1-(x+\delta)}X_xNi_\delta)$. It was found that addition of Ti and Ta leads to an increase in the lattice parameter and a decrease in the cohesive energy of $Ni_3Al$. Ni antisites cause a decrease in lattice parameter and increase in cohesive energies. Ta and Ti addition to stoichiometric $Ni_3Al$ results in an initial increase in the energies of $APB_{(111)}$, $CSF_{(111)}$, $APB_{(001)}$ and $SISF_{(111)}$. However at higher concentrations, the fault energies decrease. Addition of Ni antisites results in a monotonic decrease in the energy of all four faults. A nearest neighbor bond model was developed for $Ni_3$(Al,Ta), $Ni_3$(Al, Ti) and $Ni_3$(Al, Ni) pseudo-binary systems on the basis of which trends in fault energies were explained. The model was extended to the pseudo-ternary $Ni_3$(Al,Ta,Ni) and $Ni_3$(Al,Ti,Ni) systems. In this work, recipes were developed for predicting lattice parameters, cohesive energies and fault energies in pseudo-ternary systems on the basis of coefficients derived from simpler pseudobinary systems. The model predictions are in good agreement for lattice parameters, cohesive energies, and energies of $APB_{(111)}$ and $CSF_{(111)}$, and there is scope for refinement in the case of $APB_{(001)}$ and $SISF_{(111)}$ energies.

## References


[1] C.T. Liu, D.P. Pope, *Intermetallic compounds: principles and practice*. (John Wiley & Sons ltd, 2002) chapter2.

[2] R.C. Reed, The superalloys: Fundamentals and Applications (Cambridge University Press, 2006).

[3] B. Kear, H. Wilsdorf, "Dislocation configurations in plastically deformed polycrystalline $Cu_3Au$ alloys," *Trans Metall. Soc. AIME*, 224 (1962) 382.

[4] G.B. Viswanathan, et al., "Investigation of creep deformation mechanisms at intermediate temperatures in René 88 DT," *Acta Mater.* 53 (2005) 3041–3057.

[5] R.W. Cahn et al., "The order-disorder transformation in Ni3Al and Ni3Al-Fe alloys—I. Determination of the transition temperatures and their relation to ductility," *Acta Metall.* 35 (1987) 2737–2751.

[6] J.Y. Hwang et al., "Nanoscale Characterization of Elemental Partitioning between Gamma and Gamma Prime Phases in René 88 DT Nickel-Base Superalloy," *Metall. Met. Trans. A.* 40 (2009) 24–35.

[7] K. Muraleedharan, R. Balamuralikrishnan, and N. Das, "TEM and 3D atom probe characterization of DMS4 cast nickel-base superalloy," *J. Mat. Sci.* 44 (2009) 2218-2225.

[8] P. Hohenberg, W. Kohn, "Inhomogeneous Electron Gas," Phys. Rev. B 136 (1964) 864-871.

[9] W. Kohn, L.J. Sham, "Self-Consistent Equations Including Exchange and Correlation Effects," *Phys. Rev. A* 140 (1965) 1133-1138.

[10] G. Paolo et al., "Quantum Espresso: a modular and open-source software project for quantum simulations of materials," *J. Phys.: Condens. Matter.* 21 (2009) 395502.

[11] G. Kresse, and J. Hafner, "Ab initio molecular dynamics for open shell transistion metals," *Phys. Rev. B.* 48 (1993) 13115–13118.

[12] J.P. Perdew, K. Burke, and M. Ernzerhof, "Generalized Gradient Approximation Made Simple," *Phys. Rev. Lett.* 77 (1996) 3865–3868.

[13] M. Methfessel, and A.T. Paxton, "High-precision sampling for Brillouin-zone integration in metals," *Phys. Rev. B.* 40 (1989) 3616–3621.

[14] N.M. Rosengaard, and H.L. Skriver, "Ab initio study of antiphase boundaries and stacking faults in $L1_2$ and $DO_{22}$ compounds," *Phys. Rev. B.* 50 (1994) 4848–4858.

[15] M.H. Yoo, C.L. Fu, and J.A. Horton, "Crack-tip dislocations and fracture behavior in $Ni_3Al$ and $Ni_3Si$, *Mater. Sci. and Eng. A.*" 176 (1994) 431–437.

[16] A.F. Voter, S.P. Chen, "Accurate Interatomic Potentials for Ni, Al and $Ni_3Al$," MRS Proceedings. 82 (1986) 175.

[17] Y. Mishin, "Atomistic modeling of the γ and ′γ -phases of the Ni–Al system," *Acta Mater.* 52 (2004) 1451–1467.

[18] J. Douin, P. Veyssière, and P. Beauchamp, "Dislocation line stability in $Ni_3Al$," *Phil. Mag. A.* 54 (1986) 375–393.

[19] T. Kruml, et al., "From dislocation cores to strength and work-hardening: a study of binary $Ni_3Al$," *Acta Mater.* 50 (2002) 5091–5101.

[20] H.P. Karnthaler, E.T. Mühlbacher, and C. Rentenberger, "The influence of the fault energies on the anomalous mechanical behaviour of $Ni_3Al$ alloys," *Acta Mater.* 44 (1996) 547–560.

[21] D.M. Dimiduk, "Dislocation structures and anomalous flow in $L1_2$ compounds," *J. Phys. III . France* 1 (1991) 1025–1053.

[22] A. Korner, "Weak-beam study of superlattice dislocations moving on cube planes in $Ni_3$(Al, Ti) deformed at room temperature," *Phil. Mag. A.* 58 (1988) 507–522.

[23] M. Chandran, and S.K. Sondhi, "First-principle calculation of APB energy in Ni-based binary and ternary alloys," *Modelling Simul. Mater. Sci. Eng.* 19 (2011) 025008.

[24] N. Baluc, R. Schäublin, and K.J. Hemker, "Methods for determining precise values of antiphase boundary energies in $Ni_3Al$," *Phil. Mag. Lett.* 64 (1991) 327–334.

[25] N. Baluc, and R. Schäublin, "Weak beam transmission electron microscopy imaging of superdislocations in ordered $Ni_3Al$," *Phil. Mag. A.* 74 (1996) 113–136.

[26] F.X. Kayser, and C. Stassis, "The elastic constants of $Ni_3Al$ at 0 and 23.5 °C," *Physica Status Solidi (a).* 64 (1981) 335–342.

[27] J.R. Mihalisin, and R.F. Decker, "Phase Transformations in Nickel-Rich Nickel-Titanium-Aluminum Alloys," *Trans. Metall. Soc. AIME.* 218 (1960) 507.

[28] R.R. Hultgren, P.D. Desai, D.T. Hawkins, M. Gleiser, K.K. Kelly, Selected values of the thermodynamic properties of binary alloys, (American Society for Metals, Ohio, 1973).

[29] Y. Mishima, S. Ochiai and T. Suzuki, "Lattice parameters of Ni(γ), Ni3Al(γ′) and Ni3Ga(γ′) solid solutions with additions of transition and B-subgroup elements," *Acta Metall.* 33 (1985) 1161–1169.

[30] T.M. Pollock and A.S. Argon, "Directional coarsening in nickel-base single crystals with high volume fractions of coherent precipitates," *Acta Metall. Mater.* 42 (1994) 1859–1874.

[31] A. Heckl, et al., "The effect of Re and Ru ón γ/γ microstructure, γ-solid solution strengthening and creep strength in nickel-base superalloys," *Mater. Sci. Eng. A.* 528 (2011) 3435–3444.

[32] K.V. Vamsi and S. Karthikeyan, Communicated.

[33] M.S. Daw, S.M. Foiles and M.I. Baskes, "The embedded-atom method: a review of theory and applications," *Materials Science Reports*, 9 (1993) 251–310.

[34] C.M.F. Rae, and R.. Reed, "Primary creep in single crystal superalloys: Origins, mechanisms and effects," *Acta Mater.* 55 (2007) 1067–1081.

[35] G.L. Drew et al., eds K.A. Green et al., Superalloys 2004, (Warrendale, PA: The Mineral, Metals and Materials Society, 2004) 127–136.

[36] D. Raynor, J.M. Silcock, "Strengthening mechanisms in γ precipitating alloys," *Metal Sci.* 4 (1970) 121-129.

[37] O. Noguchi, Y. Oya, and T. Suzuki, "The effect of nonstoichiometry on the positive temperature dependence of strength of $Ni_3Al$ and $Ni_3Ga$," *Metall. Mater. Trans. A.* 12 (1981) 1647–1653.

[38] V. Paidar, D.P. Pope, and V. Vitek, "A theory of the anomalous yield behavior in $L1_2$ ordered alloys," *Acta Metall.* 32 (1984) 435–448.

[39] M.H. Yoo, "On the theory of anomalous yield behavior of $Ni_3Al$ − Effect of elastic anisotropy," *Scripta Metall.* 20 (1986) 915–920.